Electronic Supplementary Material (ESI) for Dalton Transactions.

Double single-atom MoCu Embedded Porous Carbons Boost Electrocatalytic N_2 Reduction Reaction

*Zhiya Han,[a] Chenbao Lu,[c] Senhe Huang,[c] Xinyu Chai,[c] Zhenying Chen,[c] Xintong Li,[d] Jilong Wang,[d] Jingshun Zhang, *[d] Boxu Feng,*[c] Sheng Han,*[b] Rongbin Li*[a]*

EXPERIMENTAL PROCEDURES

Chemicals and Materials.

$ZrCl_4$, $Mo(acac)_2$, $Cu(acac)_2$, 1,4-dicarboxybenzene (H_2BDC), acetic acid (HAc), N,N-Dimethylformamide (DMF), ammonium sulfate ($(NH_4)_2SO_4$), $(^{15}NH_4)_2SO_4$ with ^{15}N enrichment of 99%, Salicylic acid, Sodium citrate, Sodium hypochlorite, Sodium nitroprusside dihydrate ($C_5FeN_6Na_2O{\cdot}2H_2O$), Hydrazine hydrate, p-Dimethylaminobenzaldehyde ($C_9H_{11}NO$), Hydrochloric acid (HCl), Hydrazine dihydrochloride, 1-Propanesulfonic acid 3-(trimethylsilyl) sodium salt (DSS), dimethyl sulfoxide-d6 (DMSO-d6), None of the above-mentioned reagents require post-treatment before use.

Electrochemical testing methodology.

The electrochemical test instrument used is the CHI660E electrochemical workstation, if not otherwise specified. The electrocatalytic reactor is accomplished in an H-cell by a three-electrode system. In a typical procedure, 1 mg of catalyst and 100 μL of Nafion solution (5 wt%) were dispersed in ethanol solution via stirring for 2h. Then 100 μL of black ink was dropped on 1*1cm carbon paper. Afterward, the electrodes were dried in a vacuum oven at 40°C for 1h and purged with Ar before use. Each working electrode is guaranteed to have 1 mg of catalyst.

For experiments, the H-cell is separated by a Nafion 117 membrane. Pt wire is the counter electrode and Ag/AgCl is the reference electrode. All potentials were tested at the Ag/AgCl reference electrode and need to be converted to the relative RHE form

with the conversion equation by E (vs RHE) = E (vs Ag/AgCl) + 0.21 V + 0.0591 × pH. The electrolyte in the H-type cell is 0.1 M H_2SO_4. The electrolyte is fed with Ar for 30 min before use to remove the air from the solution, and all electrochemical catalysis is carried out for 1 h.

For flow cell experiments, the gas diffusion electrode was loaded with 1 mg of catalyst as the working electrode, Ag/AgCl as the reference electrode, and Pt wire as the counter electrode. In this case, the electrolyte flows in the peristaltic pump at a rate of 100 ml/min. In the Serpentine Airway, the flow rate of N_2 is 30 mL/min.

Measurement of ammonia.

Ammonia concentration was determined by the indophenol blue method in the experiment. In detail, 2 mL of 1 M NaOH solution containing salicylic acid (5 wt%) and sodium citrate (5 wt%) was added into 2 mL of the electrolyte after N_2 electroreduction, followed by the addition of 1 mL of 0.05 M NaClO and 0.2 mL of $C_5FeN_6Na_2O{\cdot}2H_2O$ (1 wt%). After shaking up and standing for 1 h, the concentration of NH+ 4 was measured using a UV-vis spectrophotometer at a wavelength range from 550 nm to 800 nm. The NH+ 4 shows typical absorption to ultraviolet light at the wavelength of 655 nm, in which the absorption value is in proportion to the concentration of NH+ 4. The standard concentration-absorption curve was calibrated using standard $(NH_4)_2SO_4$ solution with a serious of concentrations (0, 0.5, 1.0, 2.0, 5.0, 10.0, 20.0 μg/mL).

Measurement of N_2H_4

N_2H_4 concentration was determined by Watt and Chrisp method in the experiment. In detail, a mixture of $C_9H_{11}NO$ (5.99), HCl (12 M, 30 mL), and ethanol (30 mL) was used as a color reagent. 5 mL of the electrolyte after electrolysis was mixed with 5 mL of the color reagent. After shaking up and standing for 1 h, the concentration of N_2H_4 was measured using a UV-vis spectrophotometer at a wavelength range from 420 nm to 500 nm. The N_2H_4 show typical absorption to ultraviolet light at the wavelength of 460 nm, in which the absorption value is in proportion to the concentration of N_2H_4. The standard concentration-absorption curve was calibrated using standard hydrazine dihydrochloride solution with a serious of concentrations (0, 0.1, 0.5, 1.0, 1.5, 2.0 μg/mL).

Calculations of NH_3 yield rate

The NH_3 yield rate was calculated via the following equation:

$$R_{NH_3} = \frac{CV}{MT}$$

R_{NH3}: the yield rate of NH_3 product,

C: the measured mass concentration of NH+ 4,

V: the volume of the electrolyte (30 mL in this case),

M: the mass of the catalyst (1 mg in this case),

T: the reduction reaction time.

Calculations of FE

The FE was calculated via the following equation:

$$FE = CVNF/(QM)$$

C: the measured mass concentration of NH+ 4,

V: the volume of the electrolyte,

N: the number of electrons transferred for product formation, which is 3 for NH_3,

F: the Faraday constant, 96485 C/mol

Q: the total electric charge,

M: the relative molecular mass of NH+ 4, which is 18 g/mol.

Quantification of Ammonia via ^{1}H NMR

The isotopic labeling experiment used $^{15}N_2$ with the ^{15}N enrichment of 99% as feeding gas to clarify the source of ammonia. After ^{15}N electroreduction was conducted over material at working potential for 4h, the electrolyte was concentrated into 3 mL. Then 0.1 mL DMSO-d_6, 0.05 mL H_2SO_4 (0.05 M), and 0.1 mL DSS were added into 0.4 mL of the concentrated electrolyte. The obtained ^{15}N was identified using ^{1}H NMR spectroscopy (Bruker AVANCE AV III 600). All analyses were performed with 600 times scans.

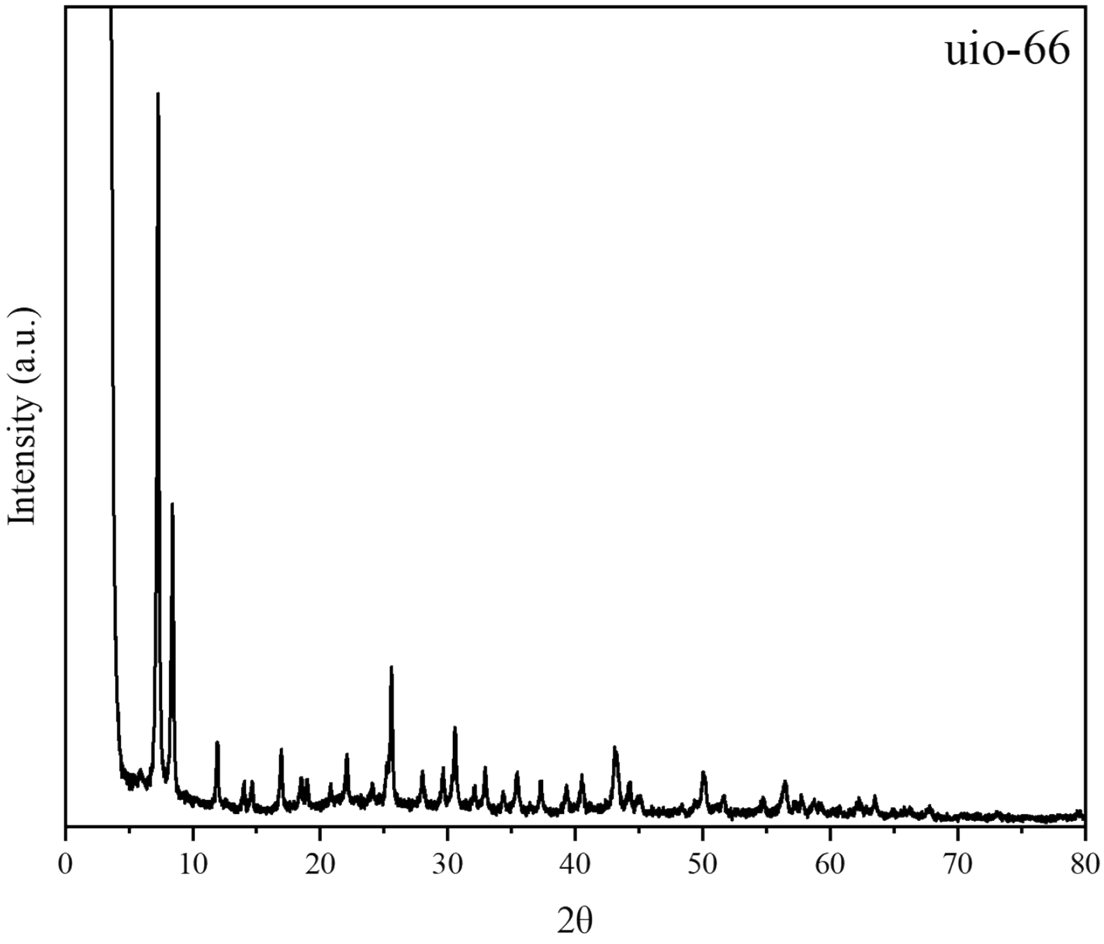

Figure S1. XRD patterns of uio-66.

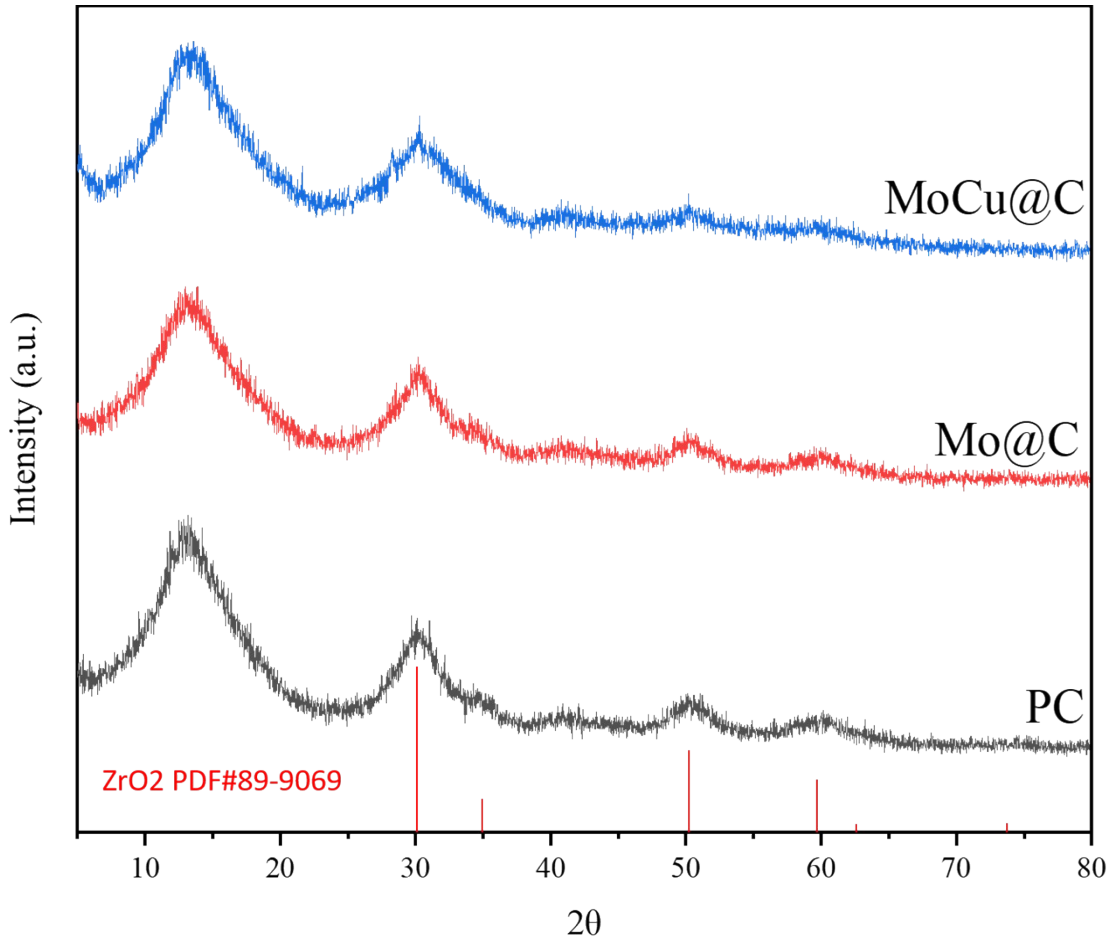

Figure S2. XRD patterns of PC, MoCu@C, and Mo@C.

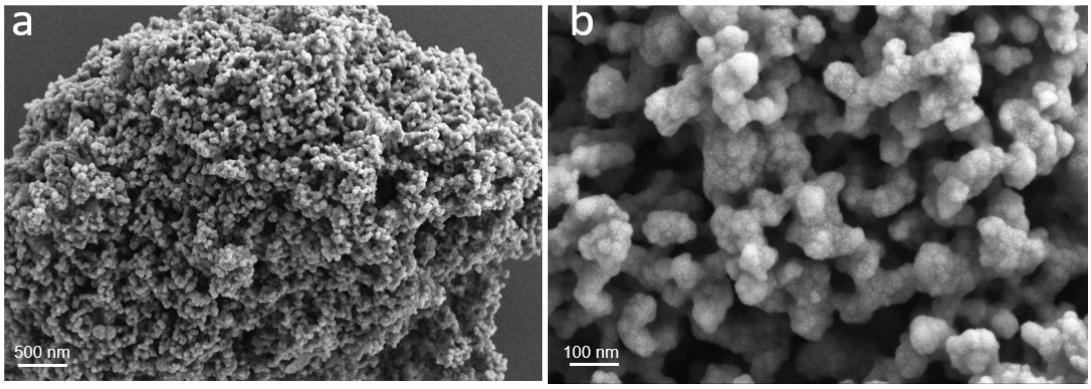

Figure S3. SEM images of MoCu@C.

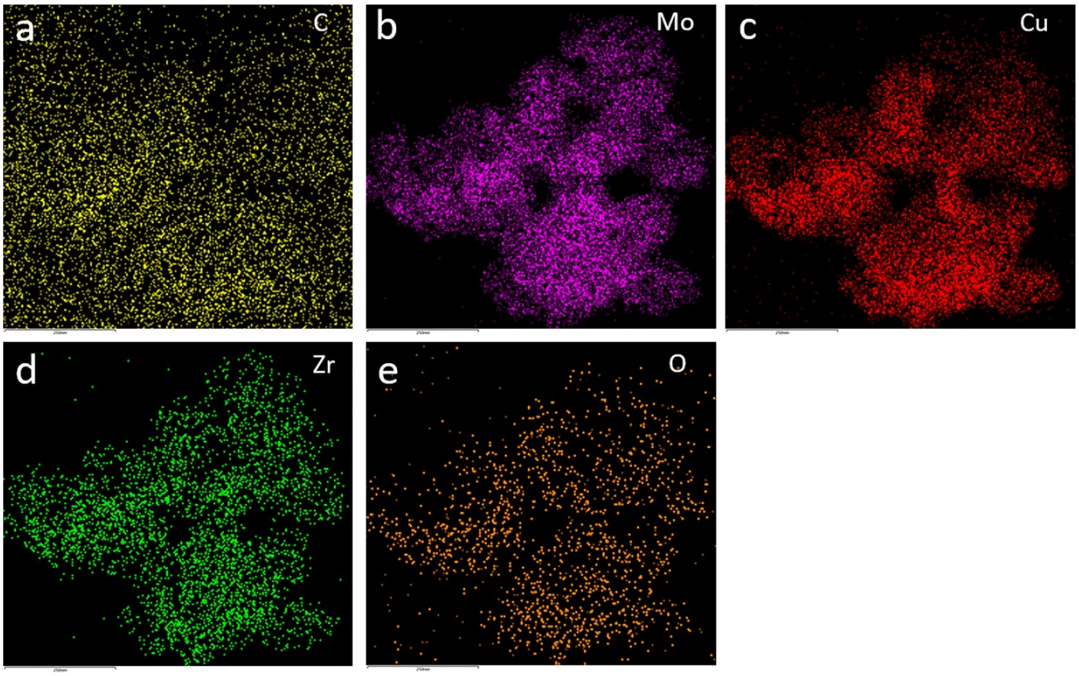

Figure S4. Corresponding EDS elemental mapping results of C, Mo, Cu, Zr, and O in MoCu@C.

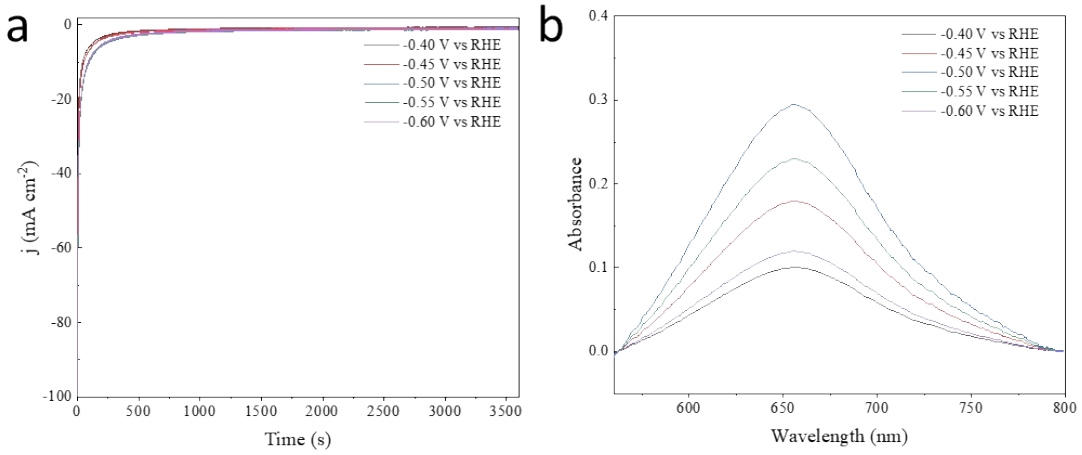

Figure S5. (a) Current densitys of MoCu@C in N_2-saturated 0.1 M H_2SO_4 at different potentials. (b) UV-Vis absorption spectra of the electrolytes MoCu@C in N_2-saturated 0.1 M H_2SO_4 at different potentials for 1h.

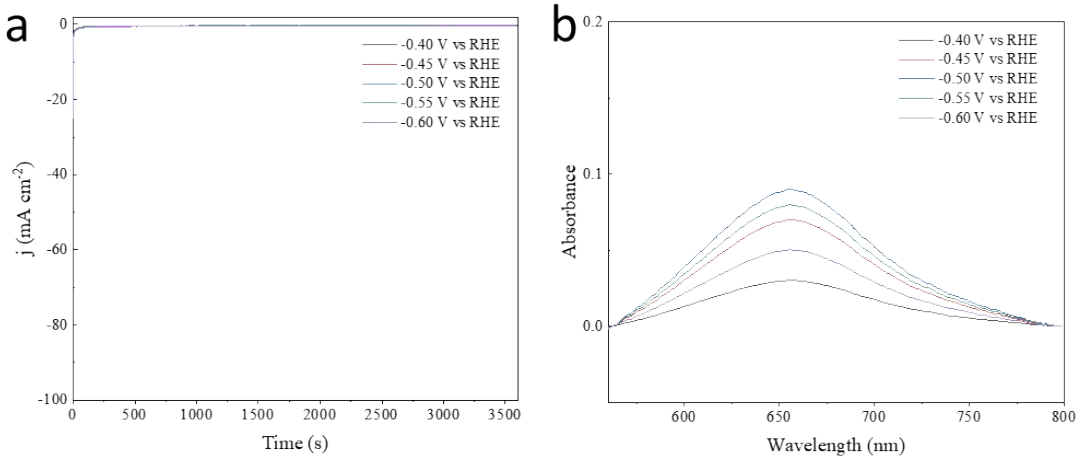

Figure S6. (a) Current densitys of Mo@C in N_2-saturated 0.1 M H_2SO_4 at different potentials. (b) UV-Vis absorption spectra of the electrolytes Mo@C in N_2-saturated 0.1 M H_2SO_4 at different potentials for 1h.

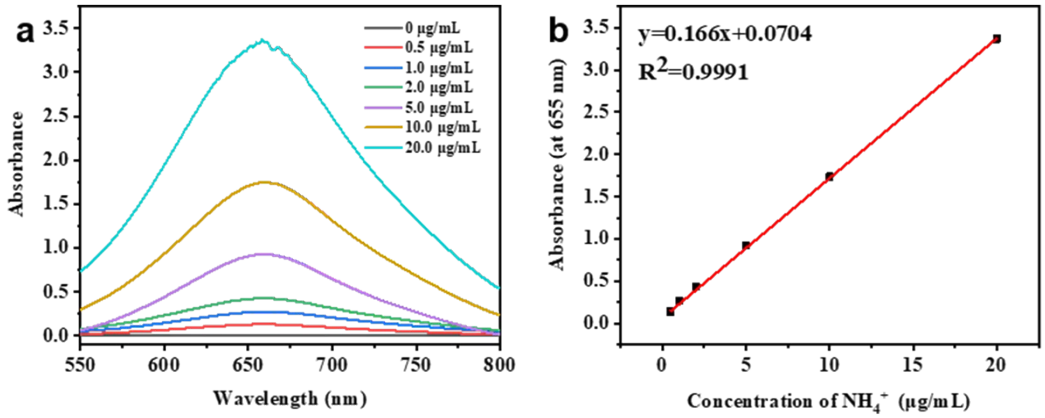

Figure S7. (a) UV-vis curves and (b) concentration-absorbance curve of NH_4^+ ions solution with a series of standard concentration. The absorbance at 655 nm was measured by UV-vis spectrophotometer. The standard curve showed good linear relation of absorbance with NH_4^+ ion concentration ($y = 0.166x + 0.0704$, $R^2 = 0.9991$).

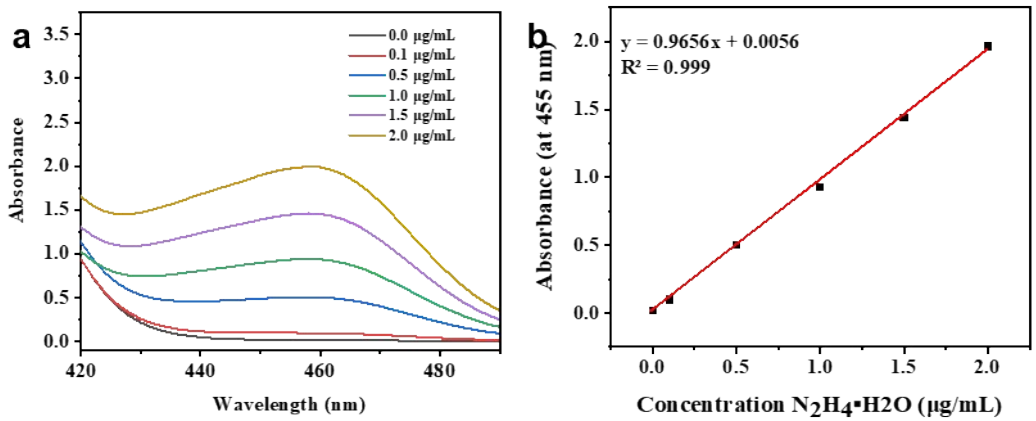

Figure S8. (a) UV-vis curves and (b) concentration-absorbance curve of N_2H_4 solution with a series of standard concentration. The absorbance at 460 nm was measured by UV-vis spectrophotometer. The standard curve showed good linear relation of absorbance with N_2H_4 concentration ($y = 0.9656x + 0.0056$, $R^2 = 0.999$).

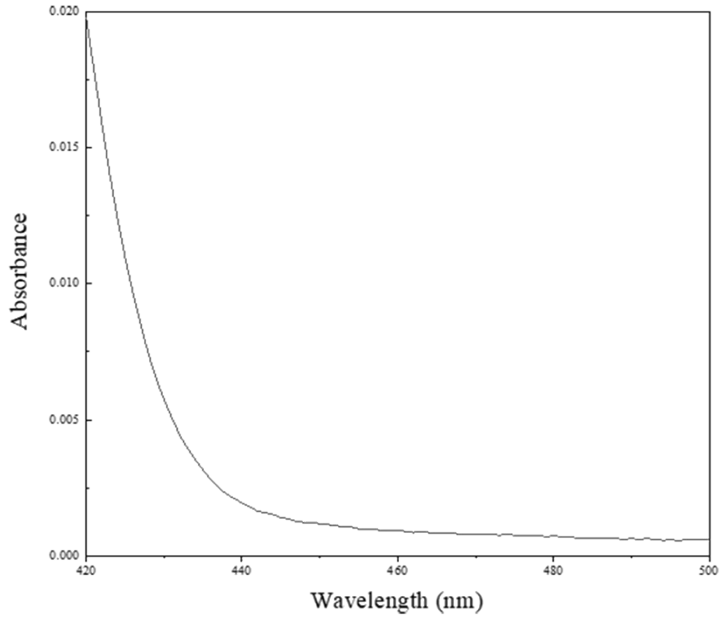

Figure S9. UV-vis absorption spectra of the electrolyte after N_2 electroreduction over MoCu@C at -0.50 V vs RHE for 1 h via Watt-and-Chrisp method. The concentration of N_2H_4 in the final electrolyte was below detection limit.

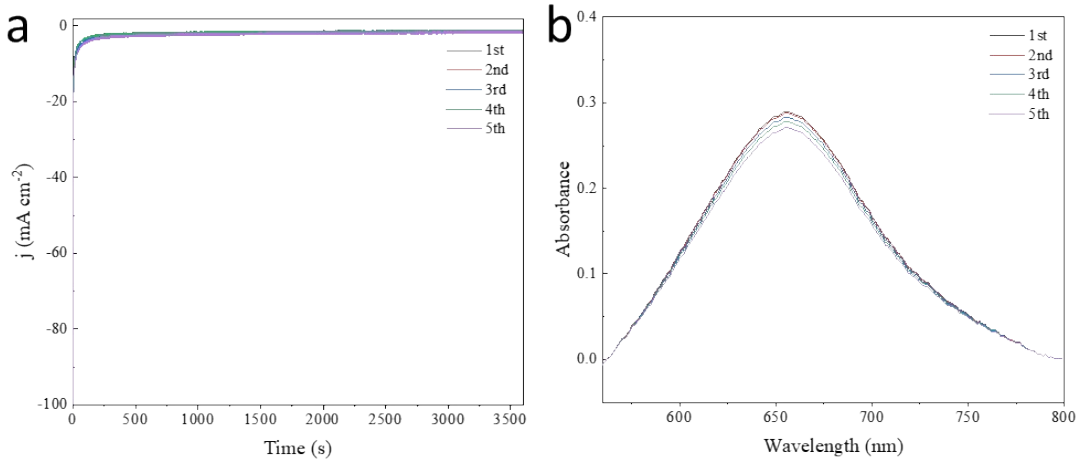

Figure S10. (a) UV-Vis absorption spectra, and (b) chronoamperometric curves of MoCu@C at −0.50 V vs RHE for 5 cycles of eNRR.

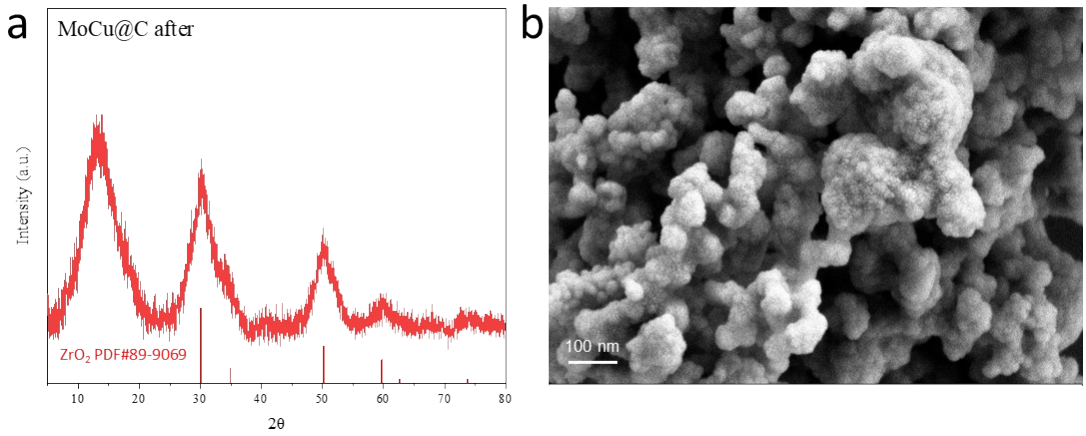

Figure S11. (a) XRD graph and (b) SEM image of the MoCu@C after eNRR durability testing.

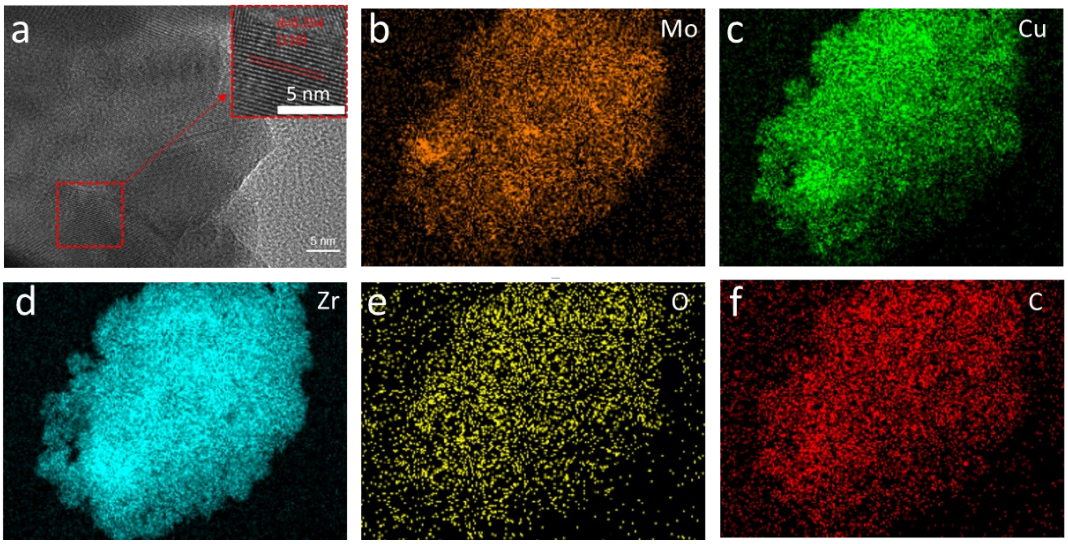

Figure S12. (a) HR-TEM image and (b-f) Corresponding EDS elemental mapping results of Mo, Cu, Zr, O, and C in MoCu@C after eNRR durability testing.

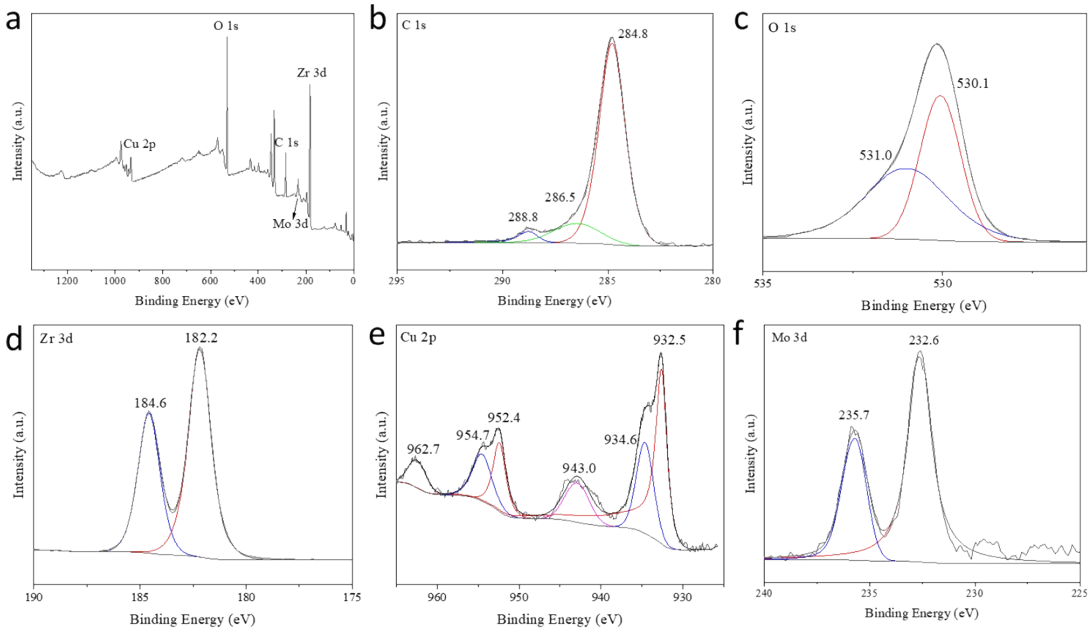

Figure S13. XPS spectra for (a) the survey scan, (b) C 1s spectra, (c) O 1s spectra, (d) Zr 3d spectra, (e) Cu 2p spectra, (f) Mo 3d spectra of MoCu@C after eNRR durability testing.

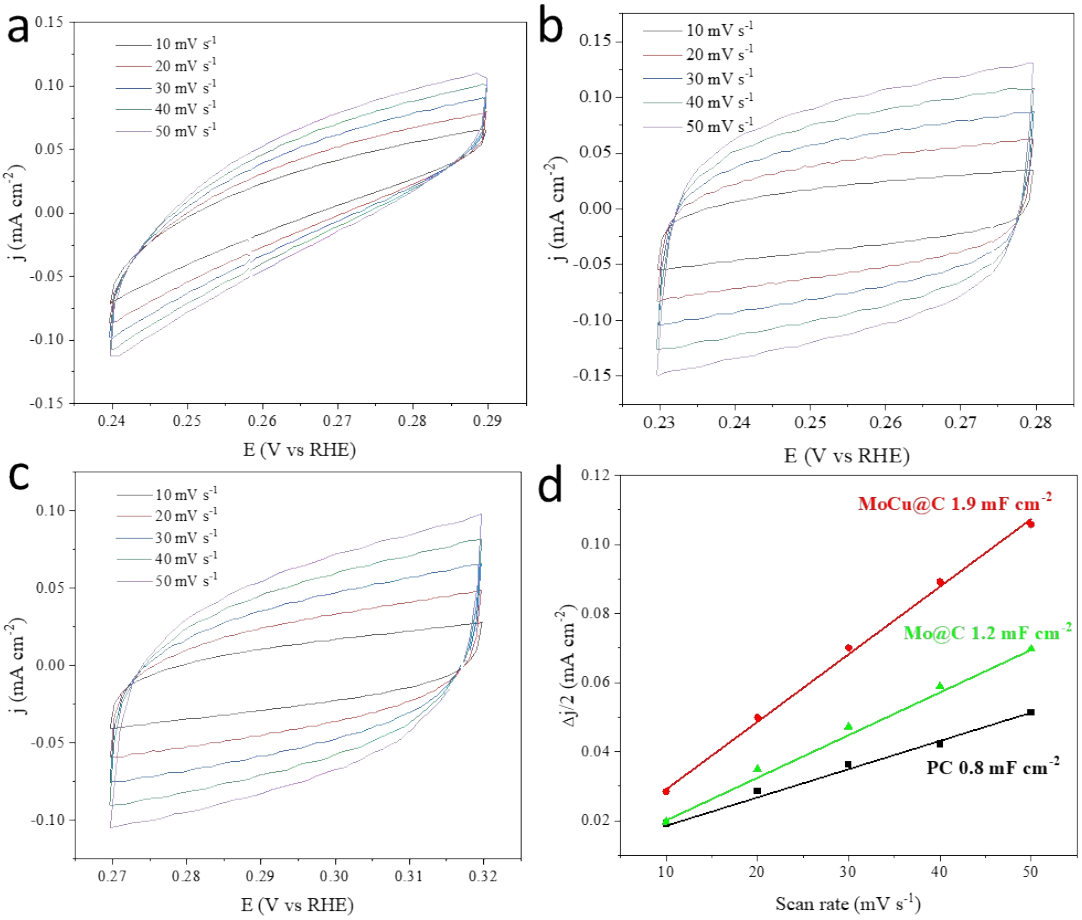

Figure S14. Cyclic voltammogram curves of (a) PC, (b) Mo@C, and (c) MoCu@C with various scan rates (10, 20, 30, 40, and 50 mV s^{-1}). (d) Charging current density differences plotted against scan rates.

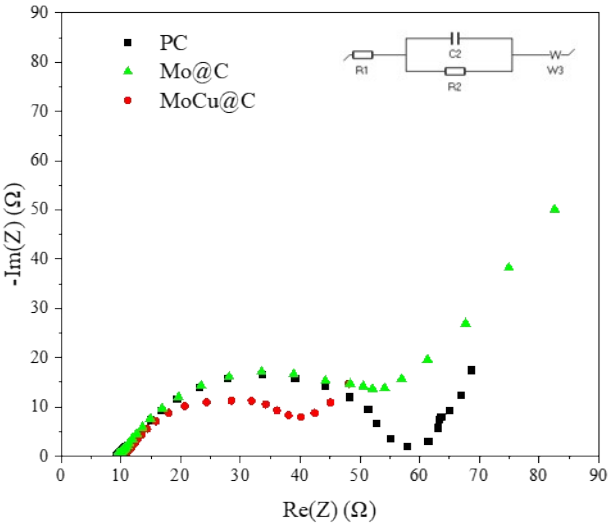

Figure S15. The Nyquist plots for EIS of PC, Mo@C, and MoCu@C.

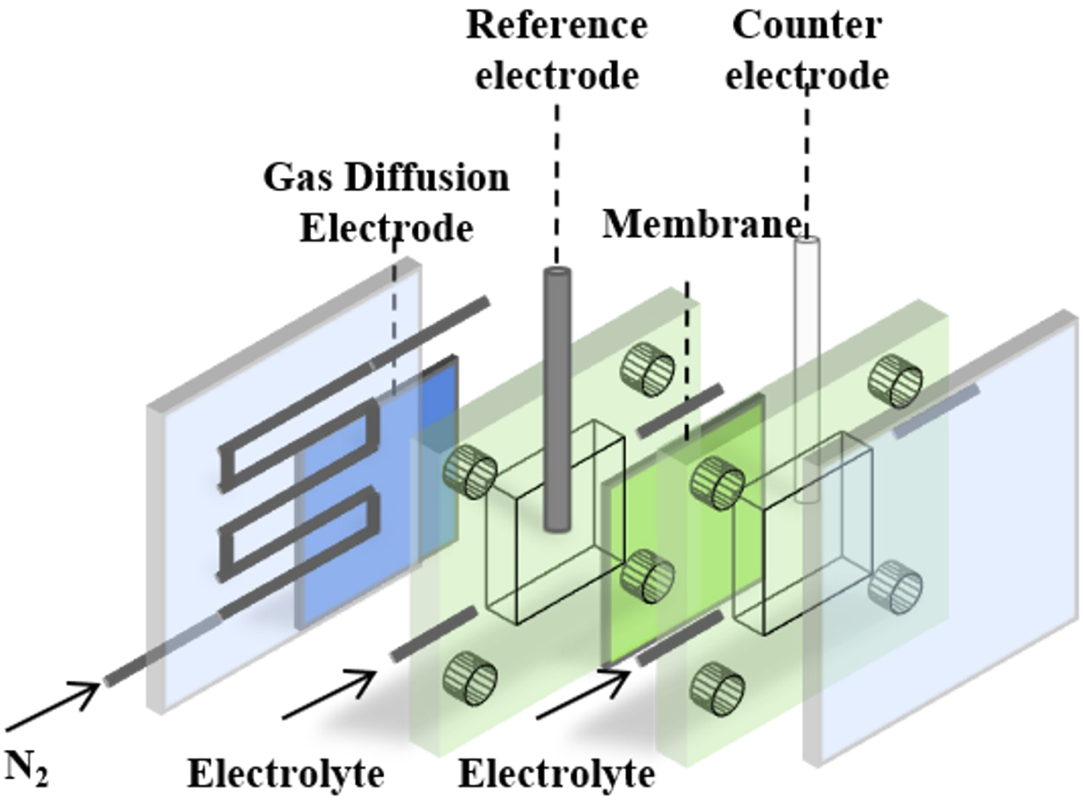

Figure S16. Schematic diagram of a flow cell.

Table S1. Summary of state-of-art catalysts for the eNRR.

Catalyst	Electrolyte	Potential	FE (%)	NH_3 yield rate	Temperature (°C)	Cell type	Reference
$Ru@ZrO_2/NC$[1]	0.1 M HCl	-0.21 *vs.* RHE	21	3.6μg h^{-1} cm^{-2}	RT	H	【1】
FeS_2-Mo[2]	0.1 M KOH	-0.2V *vs.* RHE	14.41	25.15 μg h^{-1} mg_{cat}^{-1}	RT	H	【2】
ISAS-Fe/ NC[3]	0.1 M PBS	-0.4V *vs.* RHE	18.6	62.9 μg h^{-1} mg_{cat}^{-1}	RT	H	【3】
SA-Mo/NPC[4]	0.1 M KOH	−0.3 V *vs.* RHE	14.6	34.0 μg h^{-1} mg_{cat}^{-1}	RT	H	【4】
Ru/C[5]	2 M KOH	−0.96 V *vs.* Ag/AgCl	0.92	0.25 μg h^{-1} cm^{-2}	90	PEM	【5】
Ru_2P-rGO[6]	0.1 M HCl	-0.05 V *vs.* RHE	13.04	32.8 μg h^{-1} mg_{cat}^{-1}	RT		【6】
Rh_2Sb SNRs[7]	0.5 M Na_2SO_4	-0.45 V *vs.* RHE	0.4	63.07 μg h^{-1} mg_{Rh}^{-}	RT	H	【7】
$FeMoO_4$[8]	0.5M LiClO4	−0.5V *vs.* RHE	13.2(-0.3V)	45.8 μg h^{-1} mg_{cat}^{-1}	RT	H	【8】
$W_{18}O_{49}$-16Fe@CFP[9]	0.25 M $LiClO_4$	-0.15V *vs.* RHE	20	24.7 μg h^{-1} mg_{cat}^{-1}	RT	H	【9】
a-Au/CeO_x–RGO[10]	0.1 M HCl	−0.2 V *vs.*	10.1	8.3 μg h^{-1}	RT	H	【10】

		RHE		mg_{cat}^{-1}			
Au/NCM[11]	0.1 M HCl	−0.2 V *vs.* RHE	22	36 μg h^{-1} cm^{-2}	RT	H	【11】
Amorphous $Bi_4V_2O_{11}/CeO_2$[12]	0.1 M HCl	−0.2 V *vs.* RHE	10.16	23.21 μg h^{-1} mg_{cat}^{-1}	RT	H	【12】
$IrTe_4$[13]	0.1M KOH	-0.2V *vs.* RHE	15.3	51.1 μg h^{-1} mg_{cat}^{-1}	RT	H	【13】
Te-doped C[14]	0.1M KOH	-0.5V *vs.* RHE	4.67	1.91μg h^{-1} cm^{-3}	RT	H	【14】
B-Doped graphene[15]	0.05 M H_2SO_4	−0.5V *vs.* RHE	10.8	54.88 μg h^{-1} mg_{cat}^{-1}	RT	H	【15】
BNC-NSs[16]	0.05 M H_2SO_4	-0.4V *vs.* RHE	8.1	15.7μg h^{-1} mg_{cat}^{-1}	RT	H	【16】
C@YSZ[17]	0.1M Na_2SO_4	-0.5V *vs.* RHE	8.2	24.6μg h^{-1} mg_{cat}^{-1}	RT	H	【17】
Mo@C	0.1M H_2SO_4	-0.5V *vs.* RHE	15.7 ± 0.5%	16.3 ± 1.3 μg h^{-1} mg_{cat}^{-}	RT	H	This work
MoCu@C	0.1M H_2SO_4	-0.5V *vs.* RHE	27.4 ± 0.4	52.4 ± 2.4 μg h^{-1} mg_{cat}^{-}	RT	H	This work
MoCu@C	0.1M H_2SO_4	-0.6V *vs.* RHE	7.8 ± 0.9	110.2 ± 6.5 μg h^{-1} mg_{cat}^{-}	RT	Flow cell	This work

Table S2. EIS fitting parameters for PC, Mo@C, and MoCu@C.

Event	Value	Unit	Material
R1	10.54	Ohm	MoCu@C
C2	1.827e-3	F	
R2	**19.18**	Ohm	
s3	13.06	Ohm $s^{-1/2}$	
R1	9.757	Ohm	Mo@C
C2	0.434 2e-3	F	
R2	**26.74**	Ohm	
s3	35.77	Ohm $s^{-1/2}$	
R1	10.58	Ohm	PC
C2	53.95e-6	F	
R2	**39.01**	Ohm	
s3	15.72	Ohm $s^{-1/2}$	

References

1. H. C. Tao, C. Choi, L. X. Ding, Z. Jiang, Z. S. Hang, M. W. Jia, Q. Fan, Y. N. Gao, H. H. Wang, A. W. Robertson, S. Hong, Y. S. Jung, S. Z. Liu and Z. Y. Sun, Nitrogen Fixation by Ru Single-Atom Electrocatalytic Reduction, *Chem*, 2019, **5**, 204-214.
2. H. B. Wang, J. Q. Wang, R. Zhang, C. Q. Cheng, K. W. Qu, Y. J. Yang, J. Mao, H. Liu, M. Du, C. K. Dong and X. W. Du, Bionic Design of a Mo(IV)-Doped FeS2 Catalyst for Electroreduction of Dinitrogen to Ammonia, *ACS Catal.*, 2020, **10**, 4914-4921.
3. F. Lü, S. Zhao, R. Guo, J. He, X. Peng, H. Bao, J. Fu, L. Han, G. Qi, J. Luo, X. Tang and X. Liu, Nitrogen-coordinated single Fe sites for efficient electrocatalytic N2 fixation in neutral media, *Nano Energy*, 2019, **61**, 420-427.
4. L. Han, X. Liu, J. Chen, R. Lin, H. Liu, F. Lu, S. Bak, Z. Liang, S. Zhao, E. Stavitski, J. Luo, R. R. Adzic and H. L. Xin, Atomically Dispersed Molybdenum Catalysts for Efficient Ambient Nitrogen Fixation, *Angew. Chem. Int. Ed.*, 2019, **58**, 2321-2325.
5. Y. Yao, H. J. Wang, X. Z. Yuan, H. Li and M. H. Shao, Electrochemical Nitrogen Reduction Reaction on Ruthenium, *ACS Energy Lett.*, 2019, **4**, 1336-1341.
6. R. Zhao, C. Liu, X. Zhang, X. Zhu, P. Wei, L. Ji, Y. Guo, S. Gao, Y. Luo, Z. Wang and X. Sun, An ultrasmall Ru2P nanoparticles–reduced graphene oxide hybrid: an efficient electrocatalyst for NH3 synthesis under ambient conditions, *J. Mater. Chem. A*, 2020, **8**, 77-81.
7. N. Zhang, L. Li, J. Wang, Z. Hu, Q. Shao, X. Xiao and X. Huang, Surface-Regulated Rhodium-Antimony Nanorods for Nitrogen Fixation, *Angew. Chem. Int. Ed.*, 2020, **59**, 8066-8071.
8. K. Chu, Q. Q. Li, Y. H. Cheng and Y. P. Liu, Efficient Electrocatalytic Nitrogen Fixation on FeMoO4 Nanorods, *ACS Appl. Mater. Interfaces*, 2020, **12**, 11789-11796.
9. Y. Tong, H. Guo, D. Liu, X. Yan, P. Su, J. Liang, S. Zhou, J. Liu, G. Q. M. Lu and S. X. Dou, Vacancy Engineering of Iron-Doped W18 O49 Nanoreactors for Low-Barrier Electrochemical Nitrogen Reduction, *Angew. Chem. Int. Ed.*, 2020, **59**, 7356-7361.
10. S. J. Li, D. Bao, M. M. Shi, B. R. Wulan, J. M. Yan and Q. Jiang, Amorphizing of Au Nanoparticles by CeOx -RGO Hybrid Support towards Highly Efficient Electrocatalyst for N2 Reduction under Ambient Conditions, *Adv. Mater.*, 2017, **29**, 1700001.
11. H. Wang, L. Wang, Q. Wang, S. Ye, W. Sun, Y. Shao, Z. Jiang, Q. Qiao, Y. Zhu, P. Song, D. Li, L. He, X. Zhang, J. Yuan, T. Wu and G. A. Ozin, Ambient Electrosynthesis of Ammonia: Electrode Porosity and Composition Engineering, *Angew. Chem. Int. Ed.*, 2018, **57**, 12360-12364.
12. C. Lv, C. Yan, G. Chen, Y. Ding, J. Sun, Y. Zhou and G. Yu, An Amorphous Noble-Metal-Free Electrocatalyst that Enables Nitrogen Fixation under

Ambient Conditions, *Angew. Chem. Int. Ed.*, 2018, **57**, 6073-6076.
13. J. Wang, B. Huang, Y. Ji, M. Sun, T. Wu, R. Yin, X. Zhu, Y. Li, Q. Shao and X. Huang, A General Strategy to Glassy M-Te (M = Ru, Rh, Ir) Porous Nanorods for Efficient Electrochemical N2 Fixation, *Advanced materials (Deerfield Beach, Fla.)*, 2020, **32**, e1907112.
14. Y. Yang, L. Zhang, Z. Hu, Y. Zheng, C. Tang, P. Chen, R. Wang, K. Qiu, J. Mao, T. Ling and S. Z. Qiao, The Crucial Role of Charge Accumulation and Spin Polarization in Activating Carbon-Based Catalysts for Electrocatalytic Nitrogen Reduction, *Angew. Chem. Int. Ed.*, 2020, **59**, 4525-4531.
15. X. Yu, P. Han, Z. Wei, L. Huang, Z. Gu, S. Peng, J. Ma and G. Zheng, Boron-Doped Graphene for Electrocatalytic N2 Reduction, *Joule*, 2018, **2**, 1610-1622.
16. S. Xiao, F. Luo, H. Hu and Z. Yang, Boron and nitrogen dual-doped carbon nanospheres for efficient electrochemical reduction of N2 to NH3, *Chem. Commun.*, 2020, **56**, 446-449.
17. S. Luo, X. Li, M. Wang, X. Zhang, W. Gao, S. Su, G. Liu and M. Luo, Long-term electrocatalytic N2 fixation by MOF-derived Y-stabilized ZrO2: insight into the deactivation mechanism, *J. Mater. Chem. A*, 2020, **8**, 5647-5654.